Biosensors and Bioelectronics 137 (2019) 52–57

Contents lists available at ScienceDirect

Biosensors and Bioelectronics

journal homepage: www.elsevier.com/locate/bios

Photoelectrochemical cell enhanced by ternary heterostructured photoanode: Toward high-performance self-powered cathodic cytosensing

Gao-Chao Fan[a], Yanwei Lu[a], Huan Zhao[a], Qingyun Liu[b], Zimeng Li[a], Xiliang Luo[a,*]

[a] Key Laboratory of Optic-electric Sensing and Analytical Chemistry for Life Science, MOE, Shandong Key Laboratory of Biochemical Analysis, College of Chemistry and Molecular Engineering, Qingdao University of Science and Technology, Qingdao, 266042, PR China

[b] College of Chemical and Environmental Engineering, Shandong University of Science and Technology, Qingdao, 266590, PR China

ARTICLE INFO

Keywords:
Photoelectrochemistry
Cytosensing
Self-powered sensor
Photoanode
MCF-7

ABSTRACT

Previously reported photoelectrochemical (PEC) cytosensing commonly relied on the use of photoelectrodes as both signaling sources and platforms to accommodate the biorecognition events. In such a design, the side reaction between photoelectrodes and potential reductive species in the biological media as well as the interplay between the photoelectrodes and biomolecules will inevitably impair the performance of the corresponding PEC cytosensors. Herein, we presented a facile and efficient PEC cytosensor by separating capture probe from the photoelectrode. The system is operated upon by using a ternary heterostructured photoanode to provide an evident and stable photocurrent signal, an aptamer-based biocathode for recognizing and capturing the target cells, and the corresponding signal reduction from the cell-induced steric hindrance effect. Exemplified by human breast cancer cells (MCF-7), the proposed system realizes the separation of the signaling photoanode and the sensing biocathode toward a sensitive and selective self-powered PEC MCF-7 cytosensor. This work reports a new PEC cytosensing protocol, and it is expected to attract more interest in the research of high-performance PEC cytosensing.

1. Introduction

Advanced cytosensing techniques have long been highly pursued due to the importance of cells in life science and human health [Galanzha et al., 2009; Zheng et al., 2014; Sun et al., 2016; Tang et al., 2018]. Photoelectrochemical (PEC) biosensing has recently shown its promising potential for various targets detection owning to its distinct merits of simple device, easy operation, low cost, and low background signal [Haddour et al., 2006; Zhao et al., 2015]. Of course, photoelectrode is, indeed, the core component of PEC biosensors, which produces the current detection signal when excited by the irradiation source [Gill et al., 2008; Fan et al., 2016]. The photocurrent response of the photoelectrode has a great influence on the sensitivity of the PEC biosensor, and its stability directly determines the signal stability of the PEC biosensor. Therefore, a photoelectrode with excellent PEC properties is highly desired.

Due to the importance of cytosensing and as a rapidly evolving direction of PEC bioanalysis, PEC cytosensing has recently been actively pursued by the community. Since its inception, analysts have been preoccupied with developing innovative sensing protocols for ingenious cytosensing applications [Qian et al., 2010; Zhang et al., 2011; Zhao et al., 2012a; Zhao et al., 2012b; Wu et al., 2015; Liu et al., 2015; Li et al., 2016; Pang et al., 2017; Li et al., 2018; Liu et al., 2018; Yang et al., 2018]. Principally, ideal protocols should support efficient light harvesting, proper biomolecule interfacing, as well as fast, sensitive and stable signal transduction of the cell recognition events. To this end, previous efforts have developed various PEC cytosensors. For example, graphene-CdS nanocomposites [Zhao et al., 2012b], C-dots/AuNPs nanocomposites [Liu et al., 2015], Mn-doped CdS QDs [Wu et al., 2015], TiO_2 nanoneedls@MoO_3 array [Pang et al., 2017], and conjugated polymer [Liu et al., 2018] have earlier been exploited for PEC cytosensing. However, all these protocols employ the photoelectrodes as signaling sources and simultaneously as platforms to accommodate the biomolecular probes and the subsequent cell capture events. In such a design, the side reaction between photoelectrodes and potential reductive reagents in the biologic media [Wang et al., 2014a; Wang et al., 2015; Dai et al., 2017] as well as the interplay between the photoelectrodes and biomolecules [Marmiroli et al., 2014; Li et al., 2018] will inevitably impair the performance of corresponding cytosensors. In contrast to current state-of-the-art PEC cytosensing relying on one photoelectrode, we reports herein the use of a photoanode-supported PEC cell that permit the high-performance cathodic cytosensing, with

* Corresponding author.
E-mail address: xiliangluo@qust.edu.cn (X. Luo).

https://doi.org/10.1016/j.bios.2019.04.063
Received 14 March 2019; Received in revised form 27 April 2019; Accepted 30 April 2019
Available online 03 May 2019
0956-5663/

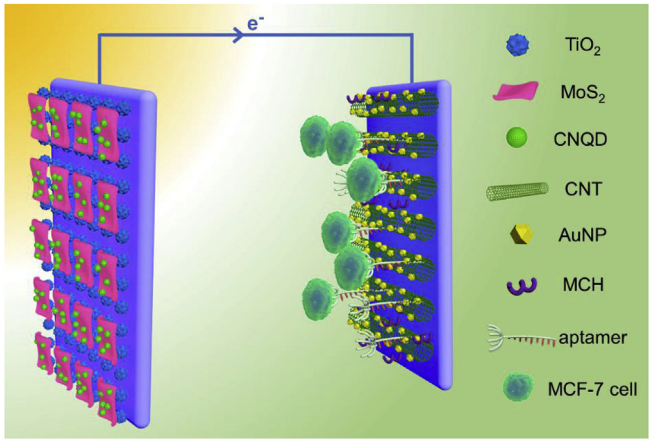

Scheme 1. The proposed self-powered photoanode-supported PEC cathodic cytosensing.

significant advantages in terms of sensitivity, selectivity, and stability.

As displayed in Scheme 1, we designed the self-powered PEC cell consisting of a light-harvesting photoanode and an aptamer-based biocathode for cytosensing, which was operated upon the signal reduction from the aptamer-induced specific cell recognition. Specifically, TiO_2 nanoparticles, MoS_2 nanosheets, and carbon nitride quantum dots (CNQDs) were modified sequentially on a bare indium–tin oxide (ITO) electrode to form the CNQDs/MoS_2/TiO_2/ITO ternary heterostructured photoanode for stable generation of the photocurrent. Meanwhile, to accommodate the biomolecules on the cathode, carbon nanotubes (CNTs) and Au nanoparticles (AuNPs) modified ITO (AuNPs/CNTs/ITO) electrode was prepared as the cathodic matrix for the aptamer immobilization and 6-mercaptohexanol (MCH) blocking. Human breast cancer cells (MCF-7) were selected as the targets, since accurate detection toward them could offer a great help to early diagnosis and treatment of breast cancer [Wu et al., 2012; Arya et al., 2013]. Exemplified by MCF-7, the designed protocol realized the separation of the signaling photoanode and the sensing biocathode toward the sensitive and selective PEC cytosensing. This work presented a new protocol for PEC cytosensing and we hope it could provide a different perspective for the development and implementation of advanced PEC cytosensing.

2. Experimental

2.1. Materials and reagents

ITO electrodes (type JH52, ITO coating 30 ± 5 nm, sheet resistance ≤ 10 Ω/square) were purchased from Beijing Zhongjingkeyi Technology Co., Ltd. (China). TiO_2 powder (P25) and carbon nanotubes (CNTs) were supplied by Alfa Aesar (China). Sodium citrate, chloroauric acid ($HAuCl_4{\cdot}4H_2O$) and ethanol were bought from Shanghai Chemical Reagent Co. (China). Sodium molybdate ($Na_2MoO_4{\cdot}2H_2O$), thioacetamide (TAA), poly(diallyldimethylammonium chloride) (PDDA, 20 wt%), and 6-mercapto-1-hexanol (MCH) were ordered from Sigma-Aldrich (USA). Ascorbic acid (AA) and urea were purchased from Sinopharm Chemical Reagent Co., Ltd (China). All other reagents were used as received. All aqueous solutions were prepared with deionized water (DI water, 18 MΩ/cm) obtained from a Milli-Q water purification system.

The used oligonucleotides were synthesized and HPLC-purified by Sangon Biotech Co., Ltd (Shanghai, China) with the following sequences: aptamer probe of MCF-7 cell, 5′-SH-$(CH_2)_6$-GCA GTT GAT CCT TTG GAT ACC CTG G-3'.

2.2. Apparatus

Scanning electron microscopy (SEM) was carried out on a Hitachi S-4800 scanning electron microscope (Hitachi Co., Japan). High-resolution transmission electron microscopy (HRTEM) was performed with a JEM-2100 transmission electron microscope with an accelerating voltage of 200 kV (Hitach, Japan). The UV–visible (UV–vis) absorption spectra were tested on a UV-3600 UV–visible spectrophotometer (Shimadzu, Japan). Confocal fluorescence imaging was performed on a confocal laser scanning microscope (LEICA TCS SP5, Germany). Photoluminescence (PL) spectra were recorded on a RF-5301PC spectrofluorophotometer (Shimadzu, Japan). A 150 W xenon lamp was utilized as the irradiation source of the photoelectrochemical test with light intensity of 500 mW/cm^2 estimated by a radiometer (Photoelectric Instrument of Beijing Saifan Co., LTD.). Photocurrent was measured on a CHI 760D electrochemical workstation (Shanghai Chenhua Apparatus Corporation, China). Electrochemical impedance spectroscopy (EIS) was carried out on an Autolab potentiostat/galvanostat (PGSTAT 30, Eco Chemie B.V., Utrecht, Netherlands) with a three-electrode system in 0.1 M KCl solution containing 5.0 mM $K_3[Fe(CN)_6]/K_4[Fe(CN)_6]$ (1:1) mixture as a redox probe, and recorded in the frequency range of 0.01 Hz–100 kHz with an amplitude of 50 mV.

2.3. Cell culture

The cells involved (MCF-7, HeLa, and HepG2), which were obtained from Procell Life Science &Technology Co., Ltd. (Wuhan, China), were cultured in an RPMI-1640 medium (Gibco, Grand Island, NY) supplemented with 10% fetal bovine serum (FBS), streptomycin (100 μg/mL), and penicillin (100 μg/mL) at 37 °C under 5% CO_2 atmosphere. At logarithmic growth phase, the cells were collected and separated from the medium by centrifugation at 1000 rpm for 5 min, and then washed with Dulbecco's phosphate-buffered saline (D-PBS). The cell sediment was resuspended in D-PBS to acquire a homogeneous suspension. The cell number was determined by a Petroff–Hausser cell counter.

2.4. Synthesis of CNQDs

The carbon nitride quantum dots (CNQDs) were synthesized according to reported literature [Zhou et al., 2013]. Typically, 0.101 g (1.68 mmol) urea and 0.081 g (0.28 mmol) sodium citrate were mixed in an agate mortar and ground to a uniform powder. The mixture was then placed in an autoclave and heated to 180 °C for 1 h. The yellowish product obtained was purified by washing with ethanol and centrifugation at 12,000 rpm, and then dialyzing against DI water through a dialysis membrane for 24 h.

2.5. Preparation of CNQDs/MoS_2/TiO_2/ITO photoanode

A certain amount of TiO_2 powder was dispersed ultrasonically in DI water, and then 20 μL of this homogeneous suspension was scattered on a bare ITO electrode with a fixed area of 0.25 cm^2. After drying in air, the film was sintered at 450 °C for 30 min and then cooled down to room temperature to obtain the TiO_2/ITO electrode. In order to acquire different thicknesses of the TiO_2 film, the increasing concentrations of TiO_2 suspension were used: 0.5, 0.75, 1.0, 1.25 and 1.5 mg/mL.

The in-situ growth of MoS_2 nanosheets was based on a previously reported literature with some modification [Li et al., 2018a]. Typically, the TiO_2/ITO electrode was placed into a 20 mL Teflon-lined stainless-steel autoclave filled with 12 mL of aqueous solution containing 4 mM $Na_2MoO_4{\cdot}2H_2O$ and 12 mM TAA. The autoclave was heated at 180 °C for 24 h in an electric oven, and then rapidly cooled down to room temperature via water rinsing. The resulting electrode was washed with DI water and ethanol several times. The loading of MoS_2 on the TiO_2/ITO electrode were controlled by just changing the original concentration of $Na_2MoO_4{\cdot}2H_2O$ with other conditions unchanged.

For CNQDs modification, the MoS_2/TiO_2/ITO electrode was in order dipped into a 1% PDDA solution and the obtained CNQDs solution for 10 min of each. The film was carefully washed with DI water after each dipping step. The two-step dipping procedure was termed as "one coating". The coating process was repeated for several times to obtain the desired CNQDs/MoS_2/TiO_2/ITO photoanode.

2.6. Fabrication of cathodic cytosensor

Prior to modification, acid treatment of carbon nanotubes (CNTs) was carried out to produce functional groups such as carboxy, hydroxyl and carbonyl onto the CNTs surface and make the CNTs disperse homogeneously in water. The treatment detail was described in our previous paper [Luo et al., 2011]. Then, 40 μL of 1 mg/mL CNTs aqueous solution was gently dropped and filmed onto a bare ITO electrode with a fixed area of 0.25 cm^2. Next, gold nanoparticles (AuNPs) were electrodeposited onto the CNTs modified ITO electrode by cyclic voltammetry technique in an aqueous solution containing 0.8 mM $HAuCl_4$ and 0.4 M KNO_3. It was performed on an electrochemical workstation with a three-electrode cell: a CNTs/ITO electrode as working electrode, a Pt wire as counter electrode, and a saturated Ag/AgCl electrode as reference electrode. The potential range of the scan segments was from −0.9 V to 0.5 V, with a scan rate of 50 mV/s. After six segments of scan, the desired AuNPs/CNTs/ITO cathodic matrix was obtained.

Subsequently, 20 μL of 5.0 μM aptamer probe of MCF-7 cell pretreated by TCEP for 1 h was dropped on the AuNPs/CNTs/ITO electrode, and it was allowed to incubate at 4 °C for 12 h. After rinsed with Tris-HCl buffer (10 mM, pH 7.4) to remove unbound aptamer probe, the electrode was blocked with 20 μL of 1 mM MCH at room temperature for 1 h followed by washing with Tris-HCl buffer. Afterwards, the resulting electrode was employed as a cytosensor and was incubated with 1 mL of MCF-7 cells suspension with a certain concentration at 37 °C for 1.5 h. After removing the non-captured cells by rinsing with PBS carefully, the electrode obtained was ready for next uses.

2.7. PEC measurement

PEC experiment was conducted in a two-electrode cell: a CNQDs/MoS_2/TiO_2/ITO electrode as the photoanode, and an AuNPs/CNTs/ITO electrode modified with bioprobe as the cathodic electrode. The photocurrent test was carried out in PBS (pH 7.4, 0.1 M) containing 0.1 M ascorbic acid (AA), which acted as electron donors to the photoanode. A xenon lamp with a spectral range of 300–2500 nm was utilized as irradiation source, which illuminated only on photoanode, and it was switched on and off every 10 s. The applied voltage was 0.0 V.

3. Results and discussion

3.1. Design principle

The self-powered photoanode-supported PEC cathodic cytosensing consisted of the signaling photoanode and the sensing biocathode and its PEC mechanism is illustrated in Scheme 2. The CNQDs/MoS_2/TiO_2/ITO ternary heterostructured photoanode was utilized purely for stable generation of the photocurrent signal. TiO_2 is a wide-band gap semiconductor (~3.2 eV) with the fascinating features of high stability and good biocompatibility [Fan et al., 2014b; Zhu et al., 2016]. MoS_2 is a typical two-dimensional semiconductor nanomaterial with layered structure that ensures fast transmission of electrons, and it has a relatively narrow band gap (~1.9 eV) [Yin et al., 2014; Yan et al., 2016]. Carbon nitride (CN), an eco-friendly material, has a mild band gap (~2.7 eV), corresponding to visible light absorption [Zhou et al., 2012; Hou et al., 2013]. Because TiO_2, MoS_2 and CNQDs had different bandgap values and stepwise band edge levels [Hou et al., 2013; Yan et al., 2016; Li et al., 2017], the as-fabricated ternary heterostructured photoanode could effectively expand the spectral absorption range and

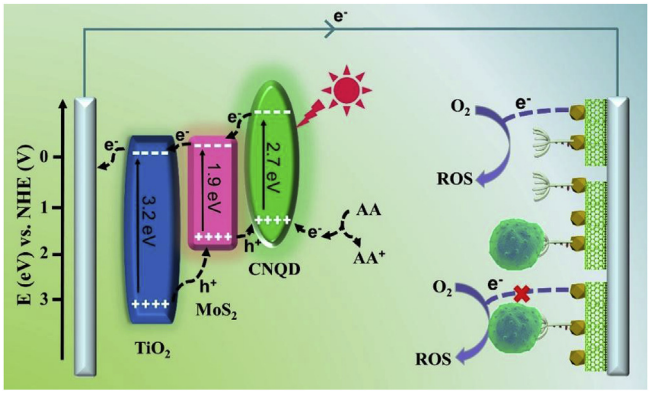

Scheme 2. PEC mechanism of the self-powered photoanode-supported PEC cathodic cytosensing.

effectively facilitate the photo-generated charge separation [Lee et al., 2010; Fan et al., 2014a]. As a result, the photocurrent signal of the ternary photoanode was dramatically improved even though no applied potential was used (namely, self-powered).

Different from previous PEC cytosensing that directly anchored biomolecules on the photoelectrode, there was no photoactive materials involved in the present sensing biocathode. Thus, only sensing biocathode was needed to incubate in target cells related biological sample. As a result, this strategy perfectly avoided the side reaction between photoanode and potential reductive species in the biological media. In addition, as the sensing biocathode involved no photoactive materials, there is no need of irradiation on the sensing biocathode, resulting in well anti-interference to excitation light and good cell activity of this kind of cytosensing. When the sensing biocathode was incubated in target-related sample, the large steric hindrance of the captured cells would hinder the electrons at biocathode interface from being captured by electron acceptor of O_2 dissolved in the electrolyte, causing obvious decrease in the current detection signal. Based on the major factors above, the target of MCF-7 cells could be detected with high sensitivity and good selectivity.

3.2. Characterizations of CNQDs and cathodic matrix

Fig. 1a shows typical TEM image of the synthesized CNQDs, from which plenty of CNQDs with average size of about 5.6 nm could be observed. The inset of Fig. 1a displays typical HRTEM image of a single CNQD. The lattice distance in the inset was found to be 0.34 nm, which was consistent with the (002) plane of hexagonal graphitic carbon nitride [Wang et al., 2014b; Wang et al., 2018]. Fig. 1b shows the UV–vis absorption and PL spectra of the CNQDs. The characteristic absorption peak of the g-CNQDs was at 344 nm in the UV–vis absorption spectrum (red line) [Zhou et al., 2013], and a narrow and symmetrical peak at 470 nm were clearly seen in fluorescence emission (blue line) with the excitation wavelength of 360 nm. The inset in Fig. 1b shows digital pictures of CNQDs solutions under white light and UV-lamp, respectively. The high brightness blue-fluorescence reflected high qualities of the synthesized CNQDs.

The successful fabrication of the AuNPs/CNTs/ITO cathodic matrix was assessed by SEM image. After CNTs were modified on the ITO electrode, as shown in Fig. 1c, plenty of disordered CNTs were successfully scattered on the ITO electrode. After AuNPs were further electrodeposited, as shown in Fig. 1d, many nanoparticles with a diameter of about 30 nm were uniformly distributed on the external surface of the CNTs.

3.3. Characterization of the photoanode

Fig. 2 exhibits SEM images of the CNQDs/MoS_2/TiO_2/ITO

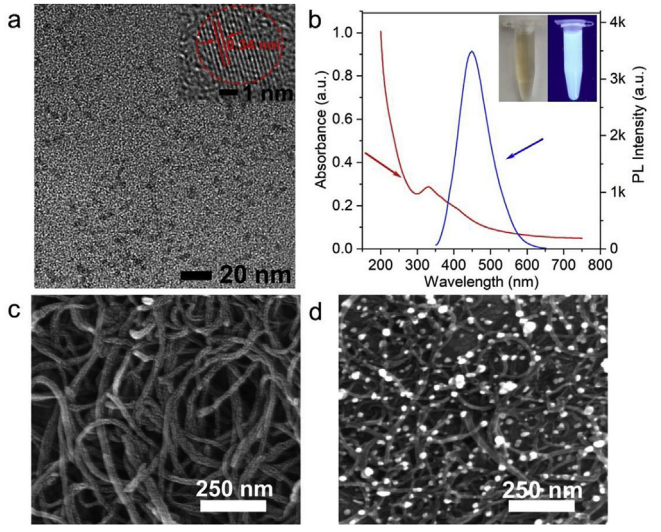

Fig. 1. (a) TEM image and (b) UV–vis absorption (red line) and PL (blue line) spectra of the CNQDs. SEM images of the (c) CNTs and (d) AuNPs/CNTs modified ITO electrodes. Inset of panel a: HRTEM image of a single CNQD. Inset of panel b: digital pictures of CNQDs solutions under white light and UV-lamp. (For interpretation of the references to colour in this figure legend, the reader is referred to the Web version of this article.)

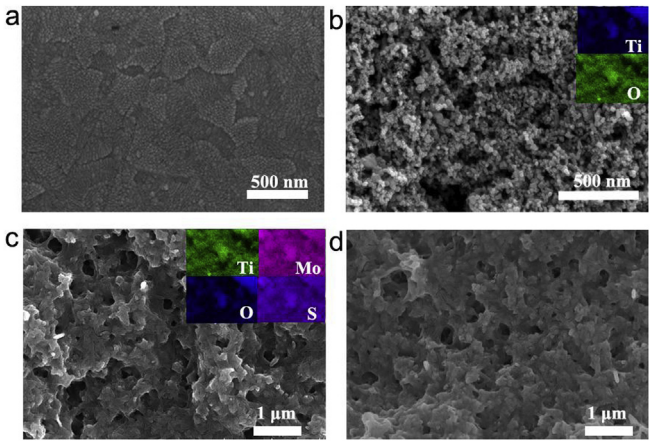

Fig. 2. SEM images of the electrodes: (a) bare ITO, (b) TiO_2/ITO, (c) MoS_2/TiO_2/ITO, and (d) CNQDs/MoS_2/TiO_2/ITO. Insets in panels b and c: elemental mapping analysis of (Ti and O) and (Ti, O, Mo, and S), respectively.

photoanode during its stepwise fabrication. The surface of the bare ITO electrode was covered with a layer of ITO nanoclusters (Panel a). After TiO_2 modification, a large number of nanoparticles with grain size of 22–28 nm was found and they formed a mesoporous film (Panel b), which increased the specific surface area of the electrode. After MoS_2 deposition, a mass of nanosheets were grown in-situ on the TiO_2 film, and the previous mesoporous surface disappeared (Panel c). After CNQDs further modification, plenty of very small particles were adhered onto the electrode and warped by a PDDA film (Panel d). In addition, the elemental mapping analysis in the inset of Panels b and c also indicated the deposition of TiO_2 and MoS_2 onto the electrode. The SEM characterization thus pointed successful fabrication of the photoanode.

3.4. PEC properties of the photoanode

For the development of high-performance PEC cytosensing, remarkable photocurrent signal and high stability of the photoanode is highly desired. Fig. 3a shows photocurrent responses of the CNQDs/

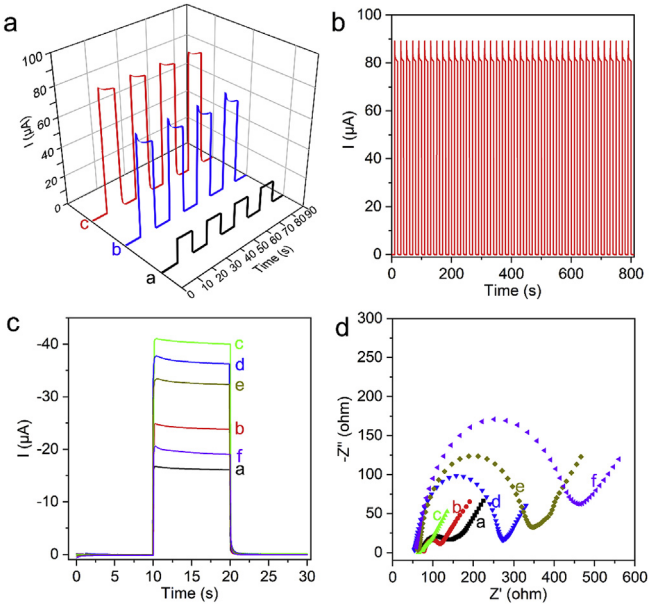

Fig. 3. (a) Photocurrent responses of the TiO_2/ITO electrode, after MoS_2 deposition, and after CNQDs modification (curves a to c, respectively). (b) Time-varying photocurrent response of the CNQDs/MoS_2/TiO_2/ITO photoanode. (c) Current signals and (d) EIS of the bare ITO as cathodic electrode, after CNTs coating, after AuNPs electrodeposition, after aptamer probe immobilization, after MCH molecules blocking, and after incubation with 5.0×10^3 cell/mL MCF-7 cells (curves a to f, respectively).

MoS_2/TiO_2/ITO photoanode during its stepwise fabrication. A Pt wire counter electrode was used for the signal measurement. The sequential modification of MoS_2 nanosheets and CNQDs resulted in obvious photocurrent enhancement. This was because the appropriate band alignment within the fabricated heterostructured photoanode could expand the spectral absorption range and promote the photo-generated charge separation, and thus inhibiting the charge recombination and improving the photocurrent intensity. The stability of the heterostructured photoanode was then investigated by its time-varying photocurrent response, as shown in Fig. 3b. Upon repeated light irradiation, the signal intensity remained almost unchanged, indicating its high stability that suitable for subsequent utilizations. Of course, the signal response of the photoanode needed to be optimized as shown in Fig. S1. The optimized photoanode was then employed to support the cathodic cytosensor development.

3.5. Characterizations of the cathodic cytosensor

The cathodic cytosensor development was first studied by current response, using the optimized photoanode as counter electrode. As shown in Fig. 3c, a weak current response was recorded on the bare ITO cathode (curve a), while the subsequent modification of CNTs and AuNPs caused obvious current enhancement that due to the improved electron transfer ability (curves b and c). After further aptamer probe immobilization and 6-mercaptohexanol (MCH) molecule blocking, moderately decreased signals were observed due to their relatively weak electron-transfer ability (curves d and e). After the cathodic cytosensor was incubated with MCF-7 cells, the photocurrent response weakened significantly (curve f), which was because that the large steric hindrance of the captured cells obstructed the electron transfer. Incidentally, the optimization on conductivity of the cathodic matrix and cell incubation time was also performed, as shown in Fig. S2.

EIS was also used to monitor the interfacial properties of the electrode along with the development of the cathodic cytosensor. As shown in Fig. 3d, the bare ITO electrode has a relatively small electron-transfer resistance (R_{et}) (curve a). After modifying CNTs, the electrode

conductivity was improved and the R_{et} was reduced (curve b). After AuNPs electrodeposition, the electrode conductivity was further improved and the R_{et} was further reduced (curve c). Aptamer probe immobilization and MCH blocking caused gradual increase of the R_{et} (curves d and e). After incubation with MCF-7 cells, the R_{et} increased obviously (curve f), indicating the target cells with large steric hindrance were captured on the sensor surface. The EIS characterization agreed with the photocurrent test of the development process of the cathodic cytosensor.

3.6. Optical monitoring of captured cells

In order to confirm the activity of the captured MCF-7 cells in the sensing process, optical imaging was conducted, as shown in Fig. S3. The MCF-7 cells captured on the cytosensor were stained with fluorescein diacetate (FDA), a widely used indicator of cell activity, which can only stain living cells. It can be seen from Panel a that the cathodic cytosensor incubated with 1.0×10^3 cell/mL of MCF-7 cells showed an obvious green FDA fluorescence, which successfully verified the activity of the MCF-7 cells captured on the sensor surface. While the cathodic cytosensor was incubated with 1.0×10^4 cell/mL of MCF-7 cells, an increased fluorescence intensity was shown in Panel b, indicating that the amount of cells captured on the sensor increased with addition of the cell concentration. Furthermore, to confirm that the MCF-7 cells were specifically bound on the cytosensor, the cathodic cytosensor without aptamer probe anchoring was used as the control to incubate with 1.0×10^4 cell/mL of MCF-7 cells, and then the fluorescence imaging was conducted. As shown in Panel c, the cytosensor without aptamer probe anchoring showed almost no green FDA fluorescence, demonstrating specific binding effect between aptamer probe and MCF-7 cell.

3.7. Sensitivity, selectivity, and stability of the cytosensor

To study analytical performance of the proposed PEC cytosensor, its current responses toward MCF-7 cells of variable amounts were recorded. The current signal of the PEC cytosensor was directly related the amount of MCF-7 cells captured on the sensor surface. As shown in Fig. 4a, with the increase of MCF-7 cell concentration in the incubation and thus captured amount of MCF-7 cells on the electrode, the photocurrent signal exhibited a gradual decrease. Fig. 4b shows the corresponding linear relationship ranging from 1.0×10^2 cell/mL to 1.0×10^5 cell/mL. The regression equation was $\triangle I = 12.33–7.05 \log C$ (cell/mL), with a correlation coefficient of 0.996. The limit of detection (LOD) was calculated to be 28 cell/mL (S/N = 3), which was lower than or comparable with those of previously reported PEC cytosensors (as shown in Table S1).

The selectivity of the PEC cytosensor was then studied by using different kinds of interfering species including HeLa and HepG2 cells at 10 times concentration of the target cells and some potential reductive reagents in the biological sample such as ascorbic acid (AA), glucose (Glu) and glutathione (GSH). As shown in Fig. 4c, a much stronger signal appeared when MCF-7 cells existed than those of HeLa and HepG2 cells as well as those small molecules, indicating good selectivity of the PEC cytosensor, mainly because the cathodic cytosensor has high affinity to target cells and good anti-interference to potential interfering reductive reagents.

The stability of the PEC cytosensor was first evaluated by its time-varying current signals. As shown in Fig. 4d, the signal intensity remained without obvious decay after more than thirty times of periodic illumination, demonstrating good stability of the designed PEC cytosensor. In addition, after the cytosensing electrode was stored at 4 °C in a refrigerator for ten days, no obvious change in current signal was found, which also reflected the good storage stability of the designed PEC cytosensor.

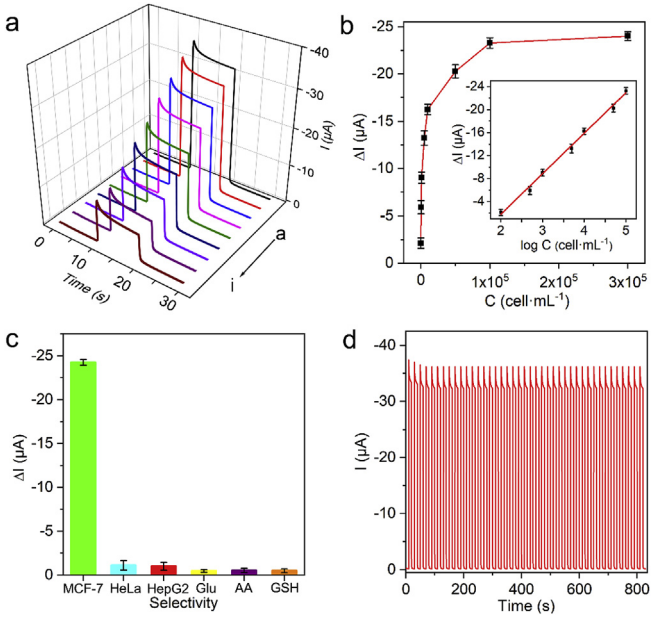

Fig. 4. (a) Current signals of the PEC cytosensor incubated with increasing concentrations of MCF-7 cells (from curve a to i); (b) plot of current change (ΔI) versus MCF-7 cell concentration; Inset of part b, calibration curve between ΔI and the logarithm of the MCF-7 cell concentration; (c) current change (ΔI) of the cytosensor toward 1.0×10^3 cells/mL MCF-7 cells, 1.0×10^5 cells/mL HeLa cells, 1.0×10^5 cells/mL HepG2 cells, 0.1 M glucose (Glu), 0.1 M ascorbic acid (AA), and 0.1 M glutathione (GSH), respectively. (d) Time-based current signals of the PEC cytosensor. $\Delta I = I_0 – I$, I_0 and I represent current signal of the PEC cytosensor before (I_0) and after (I) MCF-7 cells incubation, respectively.

4. Conclusion

This work reported the high-performance self-powered PEC cytosensing that operated upon a signaling photoanode and a sensing biocathode. In the PEC system, the photoanode was applied solely for generating an evident and stable photocurrent signal, while the biocathode was used for recognition and capture of the target cells. Based on excellent PEC properties of the CNQDs/MoS_2/TiO_2/ITO ternary heterostructured photoanode, the as-fabricated cytosensor exhibited high sensitivity with good stability for MCF-7 cells detection. In addition, due to spatial separation of the photoanode and the biocathode, this cytosensor possessed improved selectivity to resist interfering cells and reductive reagents. Such a divided protocol of PEC cytosensing offers a promising avenue for the building of self-powered PEC cytosensors toward numerous other important cells.

Declaration of interest statement

We herein declare that we have no financial and personal relationships with other people or organizations that can inappropriately influence our work, and there is no professional or other personal interest of any nature or kind in any product, service and/or company that could be construed as influencing the position presented in, or the review of, the manuscript entitled.

Acknowledgments

This work is supported by the National Natural Science Foundation of China (21603099 and 21675093), Taishan Scholar Program of Shandong Province of China (ts20110829), and State Key Laboratory of Analytical Chemistry for Life Science (SKLACLS1802).

Appendix A. Supplementary data

Supplementary data to this article can be found online at https://doi.org/10.1016/j.bios.2019.04.063.

References

Arya, S.K., Wang, K.Y., Wong, C.C., Rahman, A.R.A., 2013. Biosens. Bioelectron. 41, 446–451.
Dai, W.X., Zhang, L., Zhao, W.W., Yu, X.D., Xu, J.J., Chen, H.Y., 2017. Anal. Chem. 89, 8070–8078.
Fan, G.C., Han, L., Zhang, J.R., Zhu, J.J., 2014a. Anal. Chem. 86, 10877–10884.
Fan, G.C., Ren, X.L., Zhu, C., Zhang, J.R., Zhu, J.J., 2014b. Biosens. Bioelectron. 59, 45–53.
Fan, G.C., Zhu, H., Du, D., Zhang, J.R., Zhu, J.J., Lin, Y., 2016. Anal. Chem. 88, 3392–3399.
Galanzha, E.I., Shashkov, E.V., Kelly, T., Kim, J.W., Yang, L., Zharov, V.P., 2009. Nat. Nanotechnol. 4, 855–860.
Gill, R., Zayats, M., Willner, I., 2008. Angew. Chem. Int. Ed. 47, 7602–7625.
Haddour, N., Chauvin, J., Gondran, C., Cosnier, S., 2006. J. Am. Chem. Soc. 128, 9693–9698.
Hou, Y., Wen, Z.H., Cui, S.M., Guo, X.R., Chen, J.H., 2013. Adv. Mater. 25, 6291–6297.
Lee, Y.L., Chi, C.F., Liau, S.Y., 2010. Chem. Mater. 22, 922–927.
Li, L., Jiang, Y., Cui, C., Yang, Y., Zhang, P., Stewart, K., Pan, X., Li, X., Yang, L., Qiu, L., Tan, W., 2018a. J. Am. Chem. Soc. 140, 13335–13339.
Li, L., Zhang, Y., Zhang, L.N., Ge, S.G., Liu, H.Y., Ren, N., Yan, M., Yu, J.H., 2016. Anal. Chem. 88, 5369–5377.
Li, R., Tu, W.W., Wang, H.S., Dai, Z.H., 2018b. Anal. Chem. 90, 9403–9409.
Li, Y.H., Lv, K.L., Ho, W.K., Dong, F., Wu, X.F., Xia, Y., 2017. Appl. Catal., B 202, 611–619.
Liu, S.S., Cao, H.J., Wang, Z.Y., Tu, W.W., Dai, Z.H., 2015. Chem. Commun. 51, 14259–14262.
Liu, S.S., He, P., Hussain, S., Lu, H., Zhou, X., Lv, F.T., Liu, L.B., Dai, Z.H., Wang, S., 2018. ACS Appl. Mater. Interfaces 10, 6618–6623.
Luo, X., Weaver, C.L., Zhou, D.D., Greenberg, R., Cui, X.T., 2011. Biomaterials 32, 5551–5557.
Marmiroli, M., Pagano, L., Savo Sardaro, M.L., Villani, M., Marmiroli, N., 2014. Environ. Sci. Technol. 48, 5902–5909.
Pang, X.H., Bian, H.J., Su, M.H., Ren, Y.Y., Qi, J.N., Ma, H.M., Wu, D., Hu, L.H., Du, B., Wei, Q., 2017. Anal. Chem. 89, 7950–7957.
Qian, Z., Bai, H.J., Wang, G.L., Xu, J.J., Chen, H.Y., 2010. Biosens. Bioelectron. 25, 2045–2050.
Sun, D., Lu, J., Zhong, Y., Yu, Y., Wang, Y., Zhang, B., Chen, Z., 2016. Biosens. Bioelectron. 75, 301–307.
Tang, S., Shen, H., Hao, Y., Huang, Z., Tao, Y., Peng, Y., Guo, Y., Xie, G., Feng, W., 2018. Biosens. Bioelectron. 104, 72–78.
Wang, G.L., Liu, K.L., Dong, Y.M., Wu, X.M., Li, Z.J., Zhang, C., 2014a. Biosens. Bioelectron. 62, 66–72.
Wang, G.L., Shu, J.X., Dong, Y.M., Wu, X.M., Zhao, W.W., Xu, J.J., Chen, H.Y., 2015. Anal. Chem. 87, 2892–2900.
Wang, H., Pu, G., Devaramani, S., Wang, Y., Yang, Z., Li, L., Ma, X., Lu, X., 2018. Anal. Chem. 90, 4871–4877.
Wang, W., Yu, J.C., Shen, Z., Chan, D.K.L., Gu, T., 2014b. Chem. Commun. 50, 10148–10150.
Wu, P., Gao, Y., Zhang, H., Cai, C., 2012. Anal. Chem. 84, 7692–7699.
Wu, P., Pan, J.B., Li, X.L., Hou, X.D., Xu, J.J., Chen, H.Y., 2015. Chem. Eur J. 21, 5129–5135.
Yan, J., Chen, Z., Ji, H., Liu, Z., Wang, X., Xu, Y., She, X., Huang, L., Xu, L., Xu, H., Li, H., 2016. Chem. Eur J. 22, 4764–4773.
Yang, H.M., Zhang, Y., Zhang, L.N., Cui, K., Ge, S.G., Huang, J.D., Yu, J.H., 2018. Anal. Chem. 90, 7212–7220.
Yin, Z.Y., Chen, B., Bosman, M., Cao, X.H., Chen, J.Z., Zheng, B., Zhang, H., 2014. Small 10, 3537–3543.
Zhang, X.R., Li, S.G., Xia, J., Li, X.M., 2011. Biosens. Bioelectron. 26, 3674–3678.
Zhao, W.W., Zhang, L., Xu, J.J., Chen, H.Y., 2012a. Chem. Commun. 48, 9456–9458.
Zhao, X., Zhou, S., Jiang, L.P., Hou, W., Shen, Q., Zhu, J.J., 2012b. Chem. Eur J. 18, 4974–4981.
Zhao, W.W., Xu, J.J., Chen, H.Y., 2015. Chem. Soc. Rev. 44, 729–741.
Zheng, T., Zhang, Q., Feng, S., Zhu, J.J., Wang, Q., Wang, H., 2014. J. Am. Chem. Soc. 136, 2288–2291.
Zhou, J., Yang, Y., Zhang, C.Y., 2013. Chem. Commun. 49, 8605–8607.
Zhou, X., Jin, B., Li, L., Peng, F., Wang, H., Yu, H., Fang, Y., 2012. J. Mater. Chem. 22, 17900–17905.
Zhu, H., Fan, G.C., Abdel-Halim, E.S., Zhang, J.R., Zhu, J.J., 2016. Biosens. Bioelectron. 77, 339–346.